

RESEARCH ARTICLE

# Heterogeneity of Fractional Anisotropy and Mean Diffusivity Measurements by In Vivo Diffusion Tensor Imaging in Normal Human Hearts

Laura-Ann McGill<sup>1,2</sup>✉, Andrew D. Scott<sup>1,2</sup>✉, Pedro F. Ferreira<sup>1,2</sup>, Sonia NIELLES-Vallespin<sup>1</sup>✉, Tevfik Ismail<sup>1,2</sup>, Philip J. Kilner<sup>1,2</sup>, Peter D. Gatehouse<sup>1,2</sup>, Ranil de Silva<sup>1,2</sup>, Sanjay K. Prasad<sup>1,2</sup>, Archontis Giannakidis<sup>1,2</sup>, David N. Firmin<sup>1,2</sup>‡\*, Dudley J. Pennell<sup>1,2</sup>‡

**1** NIHR Cardiovascular Biomedical Research Unit, Royal Brompton Hospital, Sydney Street, London, SW3 6NP, United Kingdom, **2** National Heart and Lung Institute, Imperial College, London, United Kingdom

✉ These authors contributed equally to this work.

✉ Current Address: National Heart, Lung and Blood Institute, National Institutes of Health, Bethesda, Maryland, United States of America

‡ These authors also contributed equally to this work.

\* [d.firmin@imperial.ac.uk](mailto:d.firmin@imperial.ac.uk)



CrossMark  
click for updates

**OPEN ACCESS**

**Citation:** McGill L-A, Scott AD, Ferreira PF, NIELLES-Vallespin S, Ismail T, Kilner PJ, et al. (2015) Heterogeneity of Fractional Anisotropy and Mean Diffusivity Measurements by In Vivo Diffusion Tensor Imaging in Normal Human Hearts. PLoS ONE 10(7): e0132360. doi:10.1371/journal.pone.0132360

**Editor:** Alexander V Panfilov, Gent University, BELGIUM

**Received:** March 24, 2015

**Accepted:** June 14, 2015

**Published:** July 15, 2015

**Copyright:** This is an open access article, free of all copyright, and may be freely reproduced, distributed, transmitted, modified, built upon, or otherwise used by anyone for any lawful purpose. The work is made available under the [Creative Commons CC0](https://creativecommons.org/licenses/by/4.0/) public domain dedication.

**Data Availability Statement:** Data are available at <http://dx.doi.org/10.6084/m9.figshare.1463377>.

**Funding:** The research was funded by the National Institute for Health Research (NIHR) Cardiovascular Biomedical Research Unit based at Royal Brompton & Harefield Trust, Imperial College London. The funders had no role in study design, data collection and analysis, decision to publish, or preparation of the manuscript.

**Competing Interests:** The authors have read the journal's policy and have the following competing

## Abstract

### Background

Cardiac diffusion tensor imaging (cDTI) by cardiovascular magnetic resonance has the potential to assess microstructural changes through measures of fractional anisotropy (FA) and mean diffusivity (MD). However, normal variation in regional and transmural FA and MD is not well described.

### Methods

Twenty normal subjects were scanned using an optimised cDTI sequence at 3T in systole. FA and MD were quantified in 3 transmural layers and 4 regional myocardial walls.

### Results

FA was higher in the mesocardium ( $0.46 \pm 0.04$ ) than the endocardium ( $0.40 \pm 0.04$ ,  $p \leq 0.001$ ) and epicardium ( $0.39 \pm 0.04$ ,  $p \leq 0.001$ ). On regional analysis, the FA in the septum was greater than the lateral wall ( $0.44 \pm 0.03$  vs  $0.40 \pm 0.05$   $p = 0.04$ ). There was a transmural gradient in MD increasing towards the endocardium (epicardium  $0.87 \pm 0.07$  vs endocardium  $0.91 \pm 0.08 \times 10^{-3} \text{mm}^2/\text{s}$ ,  $p = 0.04$ ). With the lateral wall ( $0.87 \pm 0.08 \times 10^{-3} \text{mm}^2/\text{s}$ ) as the reference, the MD was higher in the anterior wall ( $0.92 \pm 0.08 \times 10^{-3} \text{mm}^2/\text{s}$ ,  $p = 0.016$ ) and septum ( $0.92 \pm 0.07 \times 10^{-3} \text{mm}^2/\text{s}$ ,  $p = 0.028$ ). Transmurally the signal to noise ratio (SNR) was greatest in the mesocardium ( $14.5 \pm 2.5$  vs endocardium  $13.1 \pm 2.2$ ,  $p < 0.001$ ; vs epicardium  $12.0 \pm 2.4$ ,  $p < 0.001$ ) and regionally in the septum ( $16.0 \pm 3.4$  vs lateral wall  $11.5 \pm 1.5$ ,

interests: Dudley J Pennell, Consultant to Siemens and a director of Cardiovascular Imaging Solutions. This did not alter the authors' adherence to PLOS ONE policies on sharing data and materials. The remaining authors have declared that no competing interests exist.

$p < 0.001$ ). Transmural analysis suggested a relative reduction in the rate of change in helical angle (HA) within the mesocardium.

## Conclusions

In vivo FA and MD measurements in normal human heart are heterogeneous, varying significantly transmurally and regionally. Contributors to this heterogeneity are many, complex and interactive, but include SNR, variations in cardiac microstructure, partial volume effects and strain. These data indicate that the potential clinical use of FA and MD would require measurement standardisation by myocardial region and layer, unless pathological changes substantially exceed the normal variation identified.

## Introduction

Cardiac diffusion tensor imaging (cDTI) offers novel characterisation of myocardial microstructures [1–5]. Recent technical advances in magnetic resonance (MR) hardware, combined with sequence development, have enabled reproducible in-vivo cDTI of the human heart [6–8]. The ability to interrogate the microarchitecture non-invasively has the potential to advance our understanding of diseases, such as hypertrophic cardiomyopathy, where the myocardium is reported to show disarray [9–12].

cDTI exploits the tissue specific nature of water diffusion in biological tissues, which occurs preferentially along the length of cellular structures [13,14]. From the diffusion tensor, quantitative parameters such as mean diffusivity (MD), fractional anisotropy (FA) and the helical angle (HA) can be calculated [15]. Collectively these describe the freedom of myocardial water movement, the organisation of myocardial microarchitecture, and the orientation of myocytes. Ex-vivo cDTI studies have demonstrated a close correlation between transmural DTI results and histological appearances [16–19]. Similar work in-vivo has been limited by the inherently poor signal to noise ratio (SNR) of the technique, and the challenge of detecting diffusion on a scale of  $\mu\text{m}$ , in the presence of bulk cardiac motion (on a scale of mm). Interpretation of quantitative in-vivo cDTI parameters, derived from a monopolar sequence, is further complicated by the impact of myocardial strain on the diffusion tensor [20]. Comparison with data acquired ex-vivo and using strain insensitive in-vivo acquisitions (monopolar 'sweet spot' or bipolar techniques) therefore help to contextualise results [21–22]. Moreover, in-vivo cDTI measurements are thought to include a contribution from microvascular perfusion [23–25], which in diseased myocardium may affect DTI parameters unpredictably. Further research addressing these issues is therefore required before cDTI can be clinically implemented.

Recent work in our department has sought to establish the optimal diffusion weighting for both the diffusion encoded ( $b_{\text{main}}$ ) and the reference data ( $b_{\text{ref}}$ ), with respect to myocardial characterisation with cDTI [26]. We found that elevating  $b_{\text{main}}$  from  $350\text{s}/\text{mm}^2$ , as adopted by previous studies [6,7], to  $750\text{s}/\text{mm}^2$  provided enhanced transmural image quality. Additionally we have proposed that increasing  $b_{\text{ref}}$  from  $\approx 0\text{s}/\text{mm}^2$  to  $150\text{s}/\text{mm}^2$  minimises the contribution from microvascular perfusion [26].

Although some ex vivo cDTI studies have addressed in-homogeneity in anisotropy and diffusivities [27–29], most have assumed that these measures are homogeneous; there also remains a paucity of in-vivo data in the normal heart on which to compare normal with diseased myocardium, to determine whether appreciable abnormalities exist. In this study we

describe our observations of the heterogeneity of quantitative transmural and regional cDTI, in a healthy cohort of volunteers with an optimised in-vivo sequence.

## Methods

### In-vivo Imaging Sequence

Twenty healthy volunteers (average age 32 [range 22–57], 15 male) were recruited, including data from 10 volunteers who contributed to our previous study [26]. This study was approved by the NRES Committee South East Coast Surrey (REC reference 10/H0701/112), all subjects gave written consent. Images were acquired using a 3T scanner (Magnetom Skyra, Siemens AG Healthcare Sector, Erlangen, Germany) with an anterior 18 element matrix coil and 8–12 elements of a matrix spine coil. Initial localisation images were acquired to determine the short axis of the left ventricle (LV). A mid ventricular retro-gated cine sequence, with a temporal resolution of 40ms, was then obtained to establish the timing of the subject specific end systolic pause. cDTI was acquired in a single, mid LV short axis slice during the systolic pause. Breath-hold cDTI was performed with a monopolar, diffusion-weighted stimulated echo acquisition mode (DW-STEAM) EPI sequence [6,7]. The EPI echo train was reduced with zonal excitation in the phase encode direction and GRAPPA parallel imaging [30]. The sequence is gated to every other cardiac cycle and makes the assumption that the heart position is identical on consecutive cycles. As stated above, diffusion weighting was set at  $b_{\text{main}} = 750\text{s/mm}^2$  and the  $b_{\text{ref}}$  was  $150\text{s/mm}^2$  for the separate reference data [2,26]. A minimum of eight averages were acquired at  $b_{\text{main}}$  and one at  $b_{\text{ref}}$ , with 6 diffusion encoding directions in each case. In each breath hold, 2 sets of calibration data were acquired (GRAPPA reference and EPI phase correction data, 4 cardiac cycles), followed by the standard reference images with minimal diffusion weighting ( $b = 15\text{s/mm}^2$ , 2 cardiac cycles,  $b_{\text{main}}$  only), and finally data in each of the 6 diffusion encoding directions at  $b_{\text{main}}$  or  $b_{\text{ref}}$  (12 cardiac cycles). Each breath hold was approximately 18s long and the total scan duration was approximately 20mins. The echo time (TE) was set at 24ms and the remaining sequence parameters were as described previously [6,7], with fat saturation, repetition time (TR) 2 cardiac cycles, field of view  $360 \times 135\text{mm}^2$ , slice thickness 8mm, acquired resolution  $2.8 \times 2.8\text{mm}^2$ , reconstructed resolution  $1.4 \times 1.4\text{mm}^2$ , GRAPPA factor 2, echo train length 24 and echo train duration 13ms.

To examine the impact of resolution on our results, two volunteers were scanned a second time with a higher resolution sequence. The acquired resolution was  $1.9 \times 1.9 \times 6\text{mm}$  with a TE of 37ms, an echo train length of 33 an echo train duration of 24ms, and a field of view of  $349 \times 125\text{mm}^2$ . In order to compensate for the reduced signal to noise ratio at the higher spatial resolution TR was increased to 4 cardiac cycles to allow additional T1 recovery between images and a SENSE reconstruction was used. A minimum of 8 averages were acquired with 6 diffusion encoding directions, the diffusion weighting of  $b_{\text{main}}$  and  $b_{\text{ref}}$  were unchanged, but the standard reference images had an increased diffusion weighted of  $72\text{s/mm}^2$ . Breath holds were very long, averaging 40secs, and scan time was 30mins. As only 2 individuals were scanned at this resolution, no quantitative analysis was performed, and parameter maps for HA, MD, FA & SNR results are presented for qualitative assessment.

### Diffusion tensor analysis

All cDTI was post-processed using custom-built software developed in house using MATLAB (Mathworks, MA, USA). All frames were analysed visually and those corrupted by motion were rejected. All images per subject were co-registered with a rapid multi-resolution rigid registration algorithm [31]. A rank 2 diffusion tensor was generated for each voxel and the

eigensystem (eigenvalues [e1, e2 and e2] and eigenvectors [ $\hat{e}_1, \hat{e}_2, \hat{e}_3$ ]) were then calculated for each tensor [32]. The dependence of the b-value on the heart rate was accounted for on a beat-to-beat basis in the tensor calculation. Quantitative maps of FA and MD were calculated from the eigensystem [33]. Mean intravoxel myocyte orientation was assumed to be represented by  $\hat{e}_p$  from which the myocardial HA was calculated [34]. HA gradient was calculated as described in Lombaert et al. [35], by drawing radial lines from the centre through the myocardium and using a linear regression of HA with transmural depth. The acquisition SNR before averaging was measured using the multiple acquisition method described in Reeder et al. [36], applied to the standard reference images acquired in every  $b_{\text{main}}$  breath hold ( $b = 15\text{s}/\text{mm}^2$ ). For quantitative analysis, the myocardium was divided into 3 transmural layers (endocardium, mesocardium and epicardium) using regions of interest placed at one-third and two-thirds through the myocardial wall. The myocardium was also analysed in 4 regional full thickness segments (septal, anterior, lateral and inferior). All cDTI analysis was performed by a single observer.

## Statistical analysis

The eigenvalues, MD and FA values were analysed globally, transmurally, and by segment. All values were found to be normally distributed via a visual assessment of the distributions plotted as a histogram, and are therefore shown as mean  $\pm$  standard deviation (SD). Statistical comparison was first performed using a 1-way repeated measures ANOVA followed by paired t-testing between variables using the Bonferroni correction for multiple tests. The significance level was set at  $p < 0.05$ . Due to the transmural variation in HA, values of HA gradient were only analysed globally.

## Results

cDTI was successfully performed in all subjects. The average subject RR interval and trigger times were  $917 \pm 187\text{ms}$  and  $342 \pm 91\text{ms}$  respectively.

## Helical Angle

An example HA map is shown in Fig 1. A colour coded Bullseye plot of transmural and regional helical values is shown in Fig 2. All subjects showed the expected transmural progression of average myocyte orientation from a left-handed helix in the epicardium, to circumferential in the mesocardium, to a right-handed helix in the endocardium. The average myocardial HA gradient was  $9.1 \pm 1.1^\circ/\text{mm}$ . Fig 3 shows the average regional HA line profiles for an example subject. Within the region of the mesocardium there is a subtle reduction in the rate of change of HA compared to the adjacent transmural zones.

## Fractional anisotropy

The average global FA per subject was  $0.42 \pm 0.03$ . Example quantitative FA maps are shown in Fig 4, which in 19 of 20 subjects showed circumferentially increased FA (yellow/orange) but most marked in the septal mesocardium. On transmural analysis, the FA in the mesocardium ( $0.46 \pm 0.04$ ) was greater (more anisotropic) than the endocardium ( $0.40 \pm 0.04$ ,  $p \leq 0.001$ ) and the epicardium ( $0.39 \pm 0.04$ ,  $p \leq 0.001$ ) Fig 5. There was no difference between endocardial and epicardial FA ( $p = 1.0$ ). Results for analysis of FA by LV wall are shown in Table 1. With the lateral wall as the reference ( $0.40 \pm 0.05$ ), there was no significant difference in FA between the anterior or inferior walls. In contrast, the FA in the septum was significantly greater ( $0.44 \pm 0.03$ ,  $p = 0.04$ ).

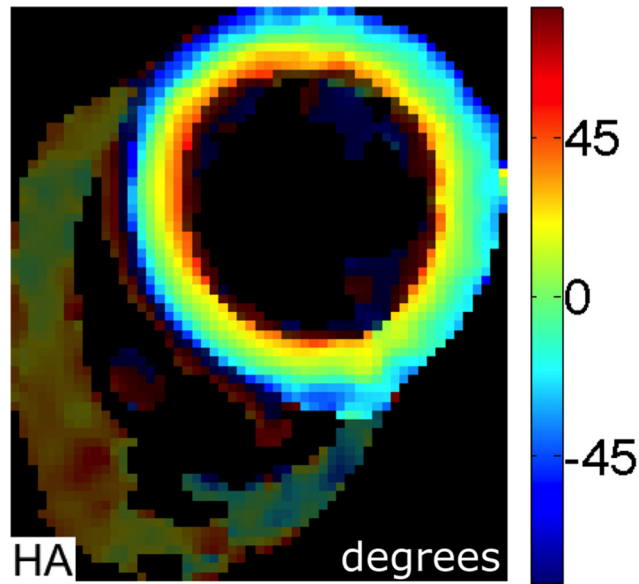


**Fig 1. Example of Helical Angle (HA) map.** This shows a smooth progression from a left-handed helical pattern in the epicardium (blue) to a circumferential orientation in the mesocardium (green) and right-handed helical pattern in the endocardium (red).

doi:10.1371/journal.pone.0132360.g001

### Mean Diffusivity

The global myocardial MD (all values  $\times 10^{-3} \text{mm}^2/\text{s}$ ) per subject was  $0.89 \pm 0.06$ . An example quantitative MD map is shown in Fig 6. Quantitative analysis showed an increase in MD transmurally (epicardium  $0.87 \pm 0.07$ ; mesocardium  $0.89 \pm 0.07$ ; endocardium  $0.91 \pm 0.08$ ) with significantly greater MD in the endocardium compared to the epicardium ( $p = 0.04$ , Fig 5).

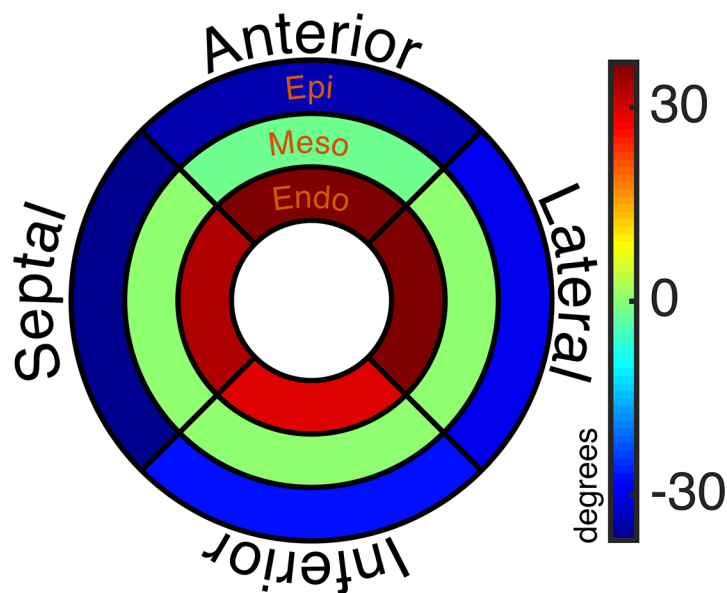


**Fig 2. Colour coded Bullseye plot of mean helical angle values per transmural layer and regional wall.** The inner, middle and outer rings represent the endo, meso and epicardium respectively. The upper, right, lower and left segments represent the anterior, lateral, inferior and septal walls respectively.

doi:10.1371/journal.pone.0132360.g002

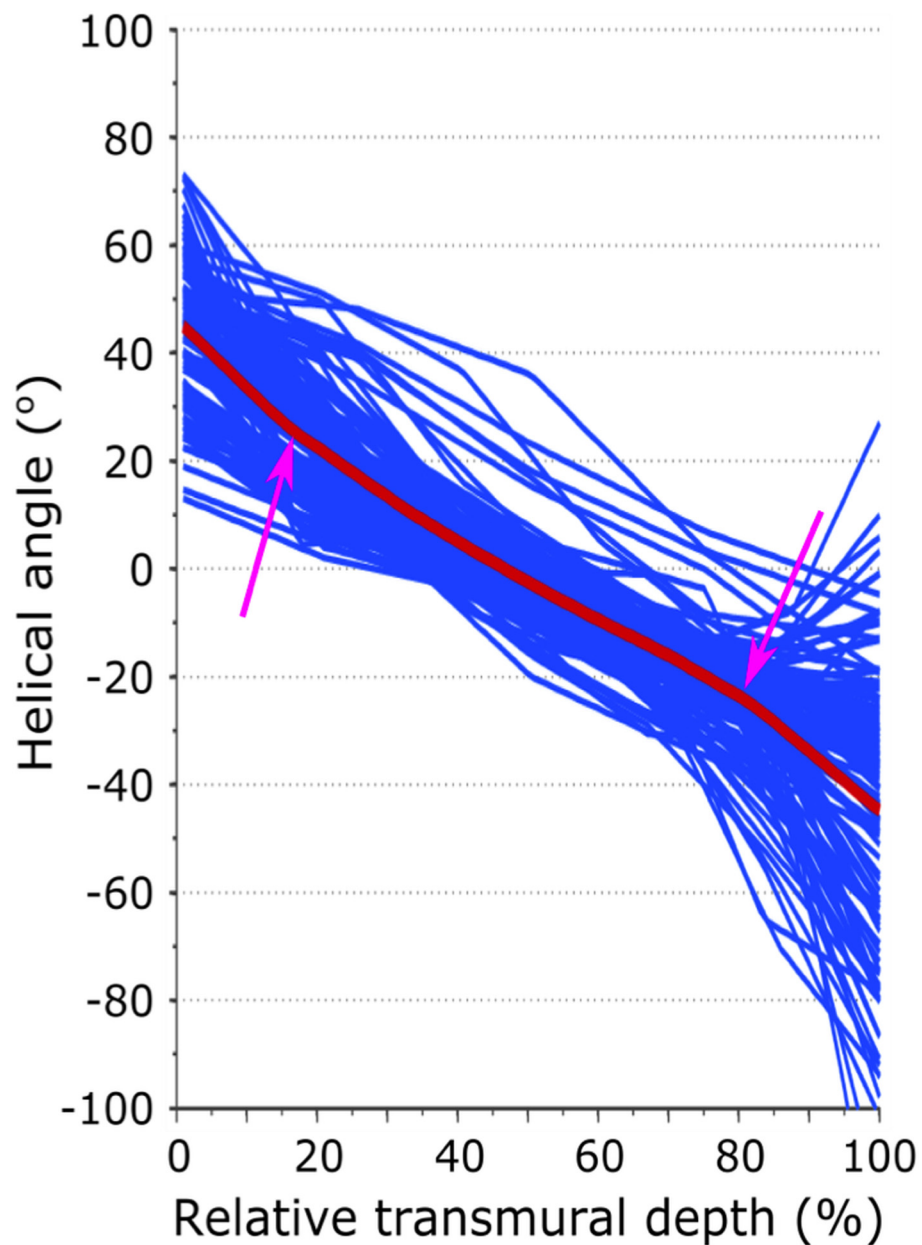


**Fig 3. Example of regional HA line profiles.** The x-axis shows the percentage distance from the endocardial surface. A relative reduction in the transmural helical angle gradient can be appreciated in the mesocardium.

doi:10.1371/journal.pone.0132360.g003

Results for regional analysis of MD are included in table 2. With the lateral wall as the reference ( $0.87 \pm 0.08$ ), MD was greater in the anterior wall ( $0.92 \pm 0.07$ ,  $p = 0.016$ ) and septum ( $0.92 \pm 0.07$ ,  $p = 0.028$ ).

### Eigenvalues

The global myocardial eigenvalues (all values in  $\times 10^{-3} \text{ mm}^2/\text{s}$ ) were:  $e1 = 1.3 \pm 0.07$ ,  $e2 = 0.85 \pm 0.08$  and  $e3 = 0.53 \pm 0.05$ . The  $e1$  in the mesocardium ( $1.33 \pm 0.08$ ) was greater than in the endocardium ( $1.28 \pm 0.09$ ,  $p = 0.001$ ) and epicardium ( $1.24 \pm 0.07$ ,  $p < 0.001$ ), and the  $e1$  in the

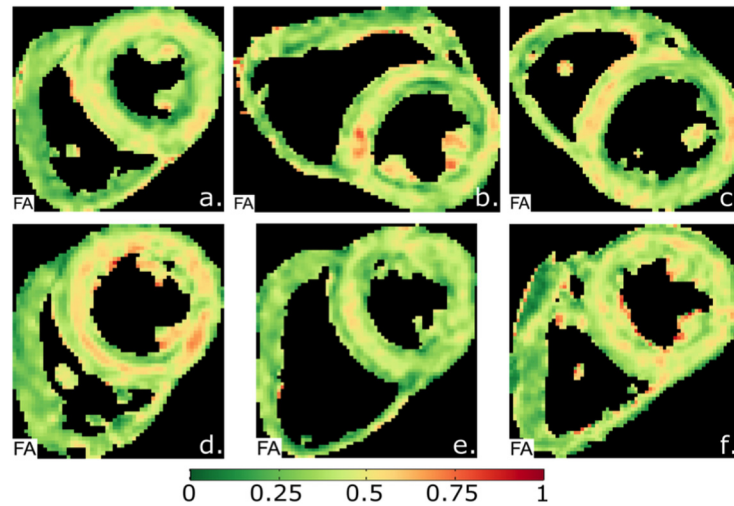


**Fig 4. Typical examples of fractional anisotropy (FA) maps.** The maps show a circumferential increase in FA (red) in the mesocardium, indicating a more anisotropic composition of myocytes compared to the endo- and epicardium.

doi:10.1371/journal.pone.0132360.g004

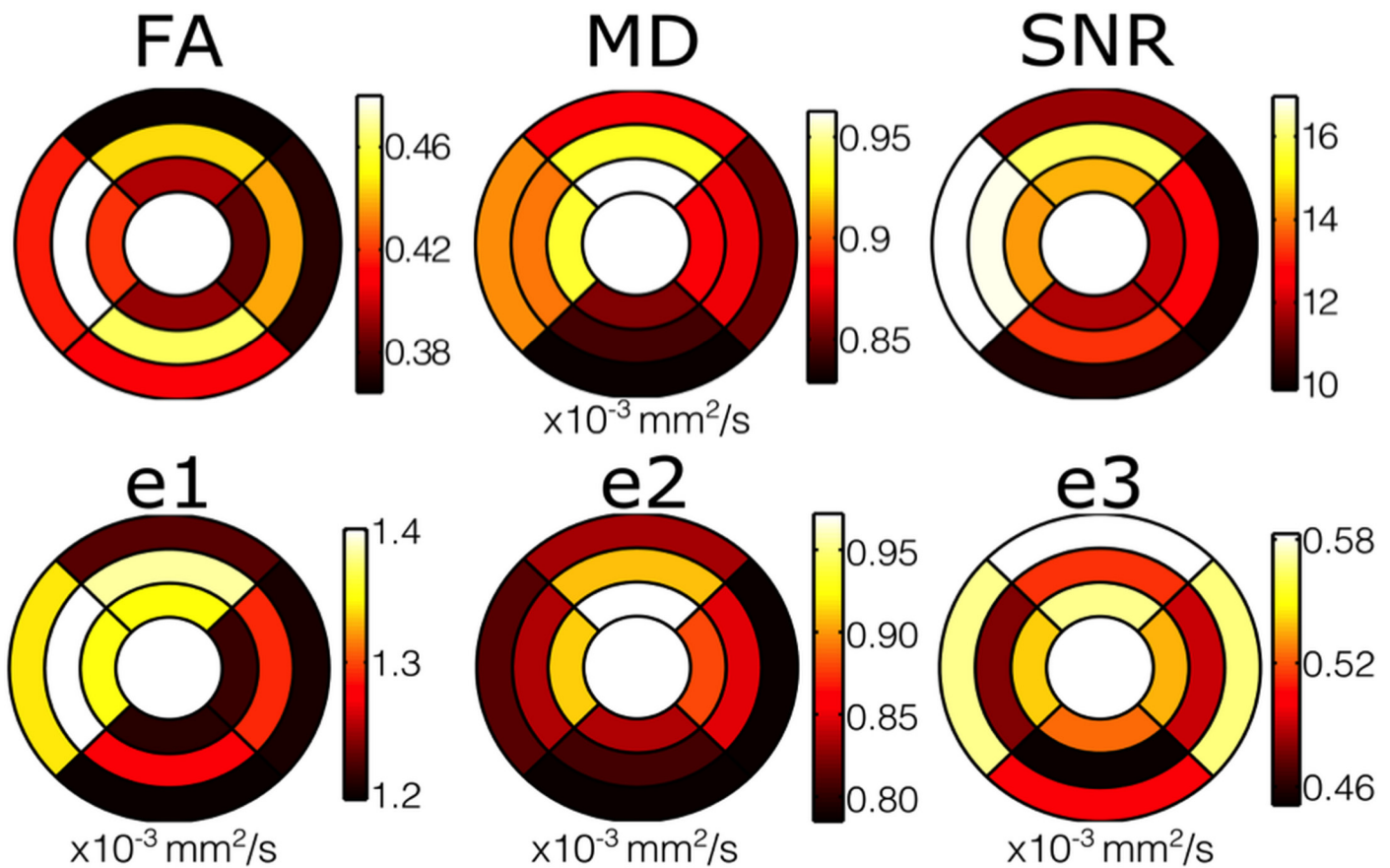


**Fig 5. Colour Bullseye maps showing the significant heterogeneity in the distribution of FA, MD, SNR and e1-e3.** The outer ring shows results from the epicardium, the middle ring shows the mesocardium, and the inner ring shows the endocardium of the single left ventricular slice. The four walls are also shown in their usual positions: Upper- anterior wall; left- septum; lower- inferior wall; right- lateral wall.

doi:10.1371/journal.pone.0132360.g005

**Table 1. Fractional Anisotropy Regional Analysis.** Lateral wall used as the reference for statistical comparisons.

FA	N	Mean	SD	Difference	95% Confidence Interval*	p value*
LV wall						
Lateral	20	0.40	0.05	Reference		
Anterior	20	0.40	0.04	-0.004	-0.030, 0.022	1.0
Inferior	20	0.42	0.05	-0.025	-0.054, 0.003	0.11
Septal	20	0.44	0.03	-0.042	-0.072, -0.012	0.04

\*Bonferroni corrected

doi:10.1371/journal.pone.0132360.t001

endocardium was greater than in the epicardium ( $p = 0.026$ , Fig 5). There was a transmural gradient in  $e_2$  from epicardium ( $0.80 \pm 0.07$ ) to mesocardium ( $0.85 \pm 0.10$ ;  $p = 0.001$ ) and endocardium ( $0.90 \pm 0.08$   $p = <0.001$ ).  $e_3$  was smaller in the mesocardium ( $0.48 \pm 0.06$ ) compared to the endocardium ( $0.54 \pm 0.07$ ,  $p < 0.001$ ) and the epicardium ( $0.55 \pm 0.07$ ,  $p < 0.001$ ), with no difference between endocardium and epicardium ( $p = 1.0$ ). Results for regional analysis of the eigenvalues  $e_1$ ,  $e_2$  and  $e_3$  are included in tables 3, 4 and 5 respectively. With the lateral wall ( $1.24 \pm 0.09$ ) as the reference,  $e_1$  was greater in the anterior wall ( $1.32 \pm 0.10$ ,  $p = 0.02$ ) and septum ( $1.37 \pm 0.08$ ,  $p < 0.001$ ). Taking the lateral wall ( $0.83 \pm 0.09$ ) as the reference,  $e_2$  was greater in the anterior wall ( $0.90 \pm 0.09$ ,  $p = 0.005$ ). There were no other statistically significant regional differences in measurements of eigenvalues were detected.

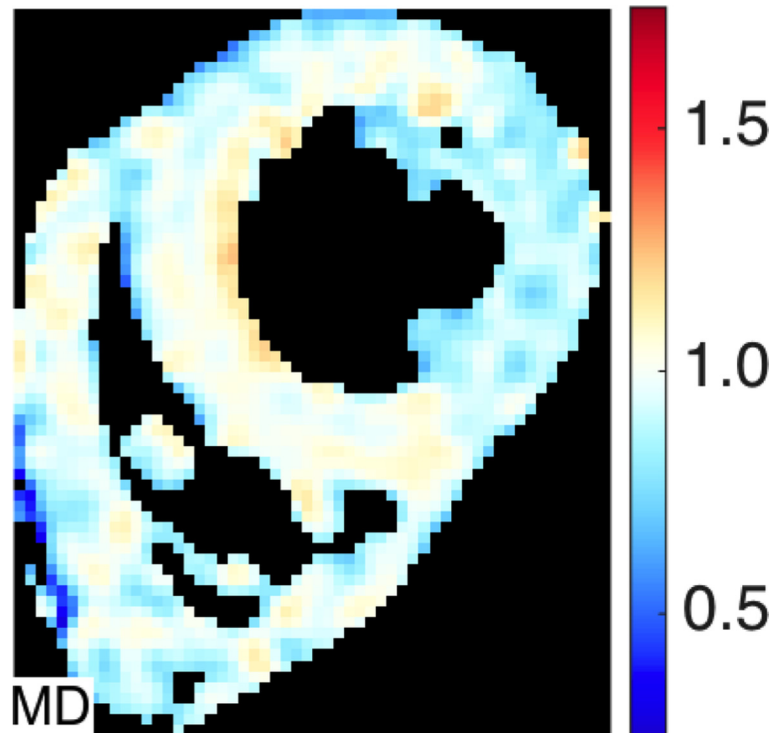


**Fig 6. Typical Mean Diffusivity (MD) map.** There is a subtle increased in the septal MD compared to the other regions.

doi:10.1371/journal.pone.0132360.g006

**Table 2. Mean Diffusivity Regional Analysis ( $\times 10^{-3} \text{mm}^2 \text{s}^{-1}$ ) Lateral wall used as the reference for statistical comparisons.**

MD	N	Mean	SD	Difference	95% Confidence Interval*	p value*
LV wall						
Lateral	20	0.87	0.08	Reference		
Anterior	20	0.92	0.08	-0.057	-0.105, -0.008	0.016
Inferior	20	0.84	0.08	0.026	-0.024, 0.076	0.89
Septal	20	0.92	0.07	-0.047	-0.091, -0.004	0.028

\*Bonferroni corrected

doi:10.1371/journal.pone.0132360.t002

## SNR

The average global myocardial SNR measured in the reference images was  $13.2 \pm 2.2$ . The SNR was greater in the mesocardium ( $14.5 \pm 2.5$ ) than the endocardium ( $13.0 \pm 2.2$ ,  $p < 0.001$ ), and epicardium ( $12.0 \pm 2.4$ ,  $p < 0.001$ , Fig 5). The results for regional wall analysis are included in table 6. With the lateral wall ( $11.5 \pm 1.5$ ) as the reference, the SNR was greater in the septum ( $16.1 \pm 3.4$ ,  $p < 0.001$ ) and anterior wall ( $14.0 \pm 3.1$ ,  $p < 0.001$ ).

## Higher Resolution Imaging

Comparative HA, MD, FA & SNR maps for both standard resolution and high resolution scans for 2 volunteers are shown in Fig 7. In both cases, the SNR maps show lower transmural SNR in the higher resolution images (global SNR 11.5 vs 15.4 in subject 1 and 8.5 vs 14.8 in subject 2), especially in the inferior and lateral walls, with worsening of the inferior wall susceptibility artefact. There was also a relative decrease in myocardial MD with the higher resolution sequence (0.82 vs 0.88 and 0.88 vs 0.93 in the two subjects) and an increase in FA (0.55 vs 0.48 and 0.51 vs 0.46). In both cases the relative increase in mesocardial FA is present at both resolutions. In regions of poor SNR, the FA is elevated.

## Discussion

### Overall findings

This cDTI study demonstrates significant transmural heterogeneity of in-vivo values of fractional anisotropy (FA) and mean diffusivity (MD) in normal human hearts. In keeping with our previous work [7], regional variations in MD were also observed, however the additional regional variation in FA is a new observation. The findings indicate that quantification of FA for clinical purposes, such as the potential use of FA to assess the myocardium for microstructural abnormalities (such as disarray) in hypertrophic cardiomyopathy, must take into account

**Table 3. E1 Regional Analysis ( $\times 10^{-3} \text{mm}^2 \text{s}^{-1}$ ). Lateral wall used as the reference for statistical comparisons.**

E1	N	Mean	SD	Difference	95% Confidence Interval*	p value*
LV wall						
Lateral	20	1.24	0.09	Reference		
Anterior	20	1.32	0.10	-0.080	-0.151, -0.010	0.019
Inferior	20	1.23	0.10	0.016	-0.054, 0.086	1.0
Septal	20	1.37	0.08	-0.13	-0.084, 0.002	$\leq 0.001$

\*Bonferroni corrected

doi:10.1371/journal.pone.0132360.t003

**Table 4. E2 Regional Analysis ( $\times 10^{-3} \text{mm}^2 \text{s}^{-1}$ ).** Lateral wall used as the reference for statistical comparisons.

E2	N	Mean	SD	Difference	95% Confidence Interval*	p value*
LV wall						
Lateral	20	0.83	0.09	Reference		
Anterior	20	0.90	0.09	-0.067	-0.070, 0.014	0.005
Inferior	20	0.81	0.10	0.027	-0.026, 0.079	0.91
Septal	20	0.85	0.09	-0.016	-0.071, 0.039	1.0

\*Bonferroni corrected

doi:10.1371/journal.pone.0132360.t004

the location and transmural extent of the region of interest from which the measurement is made. The ability to resolve the transmural variation in FA has resulted from the optimisation of cDTI which has improved the sensitivity to diffusion [26].

While the progression in helical angle (HA) is well known from both ex-vivo DTI [4,35,37], and in-vivo cDTI studies [2,4,6–8], and the FA values obtained in this work are consistent with the global values obtained in our previous work [8,26,38], the MD values are lower than those obtained in published data from Nielles-Vallespin et al. [6], ( $1.14 \pm 0.15 \times 10^{-3} \text{mm}^2/\text{s}$ ) and Tunnicliffe et al. [8], ( $1.10 \pm 0.06 \times 10^{-3} \text{mm}^2/\text{s}$ ). This can be attributed to the higher  $b_{\text{main}}$  value of  $750 \text{ s}/\text{mm}^2$  in this study, compared to  $b_{\text{main}} 350 \times 10^{-3} \text{mm}^2/\text{s}$  in prior work [6,8], combined with a  $b_{\text{ref}}$  value of  $150 \text{ s}/\text{mm}^2$ . While this protocol was found to be optimal for limiting the contribution from microvascular perfusion, one consequence of these changes is a difference in the measured cDTI parameters, including a reduction in the measured MD [26].

### Influence of microstructure on FA and MD measurements

As measured in vivo by cDTI, multiple factors are likely to contribute to FA values, including microstructural anisotropies, microstructural dynamics and possible artefacts associated with acquisition in the beating heart. Of the e1, e2 and e3 components of diffusion, the combination of high mesocardial e1 and low e3, would elevate FA in this layer. At the same time, there was an increase of e2 from epicardium to endocardium, at least in the late systolic phase investigated. One potential microstructural contributor to the FA changes could be a transmural variation in HA gradient. While the transmural variation in HA makes a layer-wise assessment of HA difficult, we did observe a small reduction in mesocardial HA gradient, which accords with the findings of ex-vivo DTI studies in canine [2] and human hearts [29]. Mesocardial e1 may therefore be elevated through a relative increase in intravoxel e1 alignment. This hypothesis is supported by histological studies which have documented a plateau in myocyte angulation within circumferentially orientated mesocardial myocytes [39,40]. Jiang et al. previously

**Table 5. E3 Regional Analysis ( $\times 10^{-3} \text{mm}^2 \text{s}^{-1}$ ).** Lateral wall used as the reference for statistical comparisons.

E3	N	Mean	SD	Difference	95% Confidence Interval*	p value*
LV wall						
Lateral	20	0.53	0.08	Reference		
Anterior	20	0.55	0.08	-0.023	-0.075, 0.029	1.0
Inferior	20	0.49	0.08	0.041	-0.014, 0.095	0.24
Septal	20	0.53	0.05	0.002	-0.042, 0.046	1.0

\*Bonferroni corrected

doi:10.1371/journal.pone.0132360.t005

**Table 6. SNR Regional Analysis.** Lateral wall used as the reference for statistical comparisons.

SNR	N	Mean	SD	Difference	95% Confidence Interval*	p value*
LV wall						
Lateral	20	11.5	1.5	Reference		
Anterior	20	14.0	3.1	-2.58	-4.10, -1.10	≤0.001
Inferior	20	11.7	2.3	-0.284	-1.33, 0.76	1.0
Septal	20	16.1	3.4	-4.64	-6.34, -2.94	≤0.001

\*Bonferroni corrected

doi:10.1371/journal.pone.0132360.t006

reported transmural heterogeneity of FA within sheep myocardium [28]. In contrast to the marked helical arrangement of human sub-epicardial myocytes, sub-epicardial myocytes in sheep are relatively more circumferentially orientated [41]. In line with our work, they similarly detected a relative increase in anisotropy within these circumferential myocytes. This was attributed to the decrease in e2 and e3 in the region, although e1 also increased but did not reach significance. One possible reason for the larger changes we observed in e1 is the longer mixing time of the DW-STEAM sequence used in our study when compared to the spin-echo sequence used by Jiang et al [28].

In addition to the well-known arrangement of myocytes from a left to a right-handed helical angle, the myocytes are also arranged in small functional units or sheetlets, separated by shear layers [42]. Sheetlets are thought to cyclically re-orientate throughout the cardiac cycle, with the shearing of the thin extracellular layers between adjacent sheetlets. This is understood to contribute to the considerable radial myocardial thickening observed in vivo [43]. LeGrice et al. measured a transmural increase in extracellular relative to intracellular volume towards the endocardium in carefully prepared canine myocardial specimens [44], and histological studies have shown the relative absence of shear layers epicardially [42,45,46]. The effects of these laminar structures on diffusion parameters have yet to be elucidated in humans, but if, as might be expected, diffusion along shear layers contributes to e2 and possibly e3, then any increase in their abundance might explain the increase in e2 from epi- to endocardium, also described by Jiang et al. [28], and also the MD gradient from epi- (lowest) to endocardium. However, the reduced e3 in the mesocardium is more difficult to explain on this basis, although it could be a reflection of a more coherent laminar structure in this layer, for instance if there was greater dominance of one, or a smaller angle between two laminar populations, as predicted in some simulations [46]. Studies documenting the electrophysiological properties of the ventricular myocardium add further support for the heterogeneity of the transmural myocardium [47]. The significant electrical differences between transmural and longitudinal cell layers may result from propagation boundaries imposed by the varying complex cellular architecture.

### Influence of strain on FA and MD measurements

Quantitative cDTI parameters acquired with monopolar sequences must be interpreted in the context of myocardial strain, which has been reported to interact with diffusion encodings [20–22]. Myocardial strain, as measured macroscopically, is maximal in the radial, cross myocyte direction and increases transmurally from the epicardium to endocardium [48]. As measurements of cDTI in this study were performed in systole, this could contribute to the gradient observed in e2, which reflects cross myocyte diffusions, however this would not appear to account for the mesocardial depression of e3 and elevation of e1 and FA. Strain

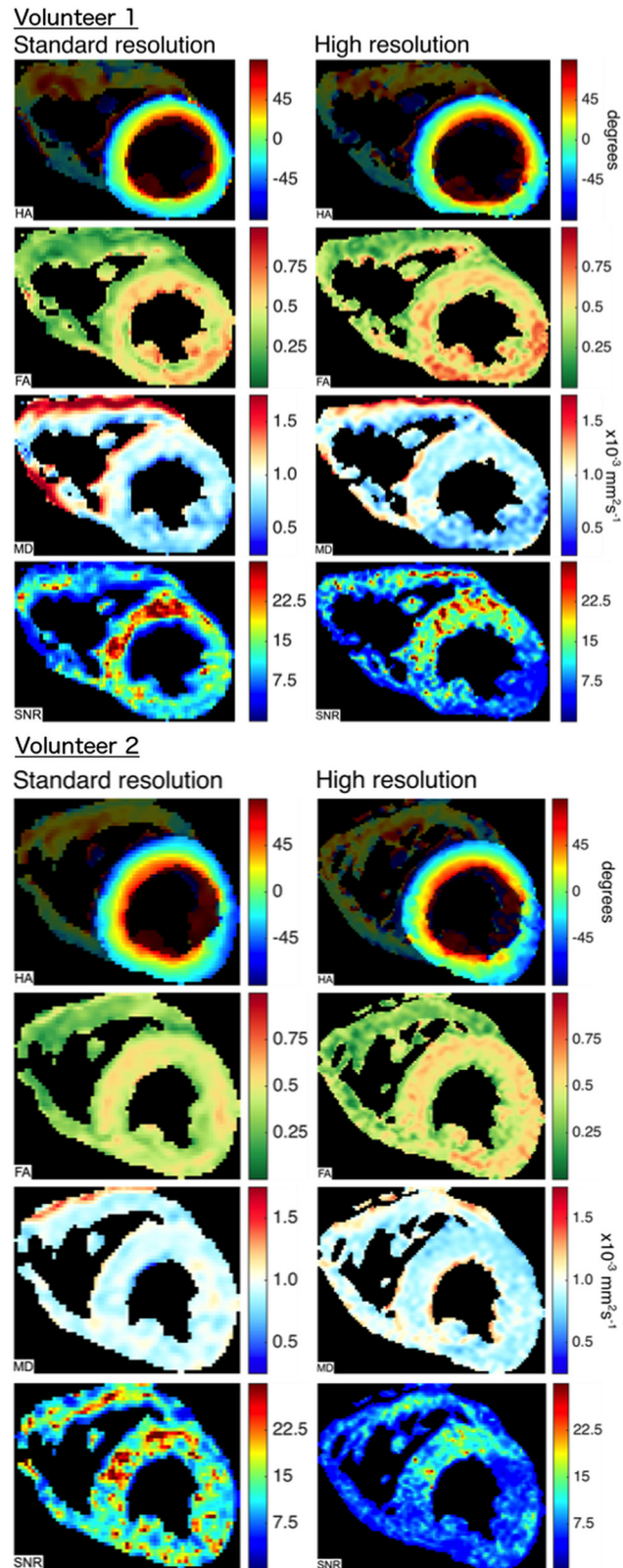


**Fig 7.** HA, FA, MD and SNR maps for 2 subjects at standard resolution ( $2.8 \times 2.8 \times 8 \text{mm}^2$ ) and higher resolution ( $1.9 \times 1.9 \times 6 \text{mm}^2$ ). In both cases the SNR is reduced in the higher resolution scan, especially in the

lateral and inferior walls. There is no difference in the transmural helical angle patterns. In regions of poor SNR in the higher resolution scans, the FA is increased and the MD is decreased. Transmurally there is little change in the FA heterogeneity between standard and higher resolution imaging.

doi:10.1371/journal.pone.0132360.g007

could also modify the MD measurement, and there is evidence for higher measured MD in systole compared with diastole [8,49]. The transmural heterogeneity of strain may also have contributed to the observed increase in endocardial MD [48].

Cardiac DTI can be acquired without strain effects. One approach is the bipolar spin echo sequence [5], however the short mixing time between winding and unwinding gradients, allows limited time for diffusion through the complex myocardial microstructure; mitigating the effects of motion during the long diffusion gradients is also challenging. An alternative strategy is to acquire cDTI data within the strain 'sweet spot' [21,22], but in practice this is difficult to define; image quality is degraded by myocardial motion; and the myocardium is comparatively thinner than systole, therefore reducing the number of pixels across the LV wall. A further option would be to undertake strain correction of the diffusion tensor; however current techniques are limited, as they make the assumption that the myocardium is an isotropic jelly like material [21,22, 50–53]. This point was illustrated in recent work by Stoeck et al. [53], which presented strain corrected cDTI data in systole and diastole acquired with the DW-STEAM EPI sequence. Post strain correction, the difference between systolic and diastolic MD appeared to increase, however as this parameter reflects the average diffusivity throughout the cardiac cycle, one would have expected the correction to eliminate the difference. [53].

### Influence of SNR on FA and MD measurements

We observed that increasing values of SNR were associated with higher values of FA both transmurally and regionally. The influence of SNR on FA and MD is difficult to predict; at low b-values, noise results in an overestimation of FA [54,55] whereas at high b-values, noise results in an underestimation of both FA and MD [54]. The transition from the low to high b-value regime depends on a number of factors including both the FA and MD of the tissue and the SNR of the acquisition. While previous work has studied these effects in the brain, and for diffusion weighted imaging generally [56], a comprehensive set of simulations with myocardium specific parameters is required to fully characterise this transition in the heart. However, in the high b-value regime, we would expect to observe that higher measurement noise levels, with lower SNR, would favour lower anisotropy. Our data showed lower FA and SNR in the epicardium & endocardium, thus we might conclude that our sequence is a high b-value regime for FA, and that SNR contributes to transmural FA heterogeneity. However, in contradiction to this possible conclusion, is that the FA maps at higher resolution (Fig 6) appear to demonstrate an increase in FA in areas of low SNR, in keeping with a low b-value regime. The observed relationship of decreasing MD regionally with low SNR is also in keeping with a high b value regime for MD. The MD pattern does not track SNR transmurally however, and other factors appear to influence these MD measurements.

### Influence of resolution and partial volume effects on FA and MD measurements

A further potential contribution to heterogeneity of FA and MD measurements is from partial volume effects, which would be most marked in the endocardium and epicardium. The potential influence could be through direct measurement aberration but also through reduced SNR. The relatively low resolution of our sequence (six pixels acquired resolution on average across

the septum) may thus have contributed to the observed heterogeneity. In an attempt to investigate this further we performed higher resolution scans in 2 subjects who were able to comply with the very long breath holds required (average 40s). The FA maps showed little difference in the pattern of heterogeneity between standard and high resolution scanning, arguing against partial voluming as a significant contributor however more subject data is required to confirm this quantitatively.

Our data demonstrates that the trade off with higher resolution is reduced SNR and increased susceptibility to artefact; this, combined with need for either prohibitively long or additional breath holds, limits the clinical application of higher resolution STEAM cDTI presently.

## Conclusions

The above consideration of factors that might influence FA and MD allows their relative non-specificity as parameters for the characterisation of myocardial structure to be appreciated. More differentiated analysis of cDTI, for example by distinguishing and appropriately analysing the values of each of the three eigenvectors of diffusion, may therefore be advantageous, although interpretation is likely to remain challenging. Using an optimised in-vivo cDTI sequence in normal subjects, we have shown significant transmural and regional variation in MD and particularly FA, which indicates that quantification of this measurement requires careful selection of the region of interest. Standardisation of the measurement method of FA and MD would be required to interpret values between studies and centres, and the possible interpretation of the presence of abnormal myocardium on a microstructural level, such as disarray, would require demonstration that the magnitude of the quantitative differences versus normal significantly exceeds these normal variations.

## Supporting Information

**S1 File. Workbook of analysed cDTI data: Excel workbook of analysed regional and transmural FA and MD data.**  
(XLSX)

## Author Contributions

Conceived and designed the experiments: LAM ADS. Performed the experiments: LAM ADS. Analyzed the data: LAM ADS. Contributed reagents/materials/analysis tools: ADS PF SNV. Wrote the paper: LAM ADS PF SNV TI PJK PDG RdS SKP AG DNF DJP. Scanned the volunteers and performed stats: LAM. Optimised the sequence & scanned the volunteers: ADS. Wrote the original sequence for our Skyra 3T scanner: SNV. Designed the software used in analysis: PF ADS.

## References

1. Edelman RR, Gaa J, Wedeen VJ, Loh E, Hare JM, Prasad P, et al. In vivo measurement of water diffusion in the human heart. *Magn Reson Med* 1994; 32: 423–8. PMID: [7984077](#)
2. Reese TG, Weisskoff RM, Smith RN, Rosen BR, Dinsmore RE, Wedeen VJ. Imaging myocardial fiber architecture in vivo with magnetic resonance. *Magn Reson Med* 1995; 34: 786–91. PMID: [8598805](#)
3. Wu MT, Tseng WY, Su MY, Liu CP, Chiou KR, Weeden VJ, et al. Diffusion tensor magnetic resonance imaging mapping the fiber architecture remodeling in human myocardium after infarction: correlation with viability and wall motion. *Circulation* 2006; 114: 1036–1045. PMID: [16940196](#)
4. Toussaint N, Stoeck CT, Schaeffter T, Kozerke S, Sermesant M, Batchelor PG. In vivo human cardiac fibre architecture estimation using shape-based diffusion tensor processing. *Med Image Anal* 2013; 17: 1243–55. doi: [10.1016/j.media.2013.02.008](#) PMID: [23523287](#)

5. Nguyen C, Fan Z, Sharif B, He Y, Dharmakumar R, Berman DS, et al. In vivo three-dimensional high resolution cardiac diffusion-weighted MRI: A motion compensated diffusion-prepared balanced steady-state free precession approach. *Magn Reson Med* 2014; 72:1257–67. doi: [10.1002/mrm.25038](https://doi.org/10.1002/mrm.25038) PMID: [24259113](https://pubmed.ncbi.nlm.nih.gov/24259113/)
6. Nielles-Vallespin S, Mekkaoui C, Gatehouse P, Reese TG, Keegan J, Ferreira PF, et al. In vivo diffusion tensor MRI of the human heart: reproducibility of breath-hold and navigator-based approaches. *Magn Reson Med* 2013; 70: 454–65. doi: [10.1002/mrm.24488](https://doi.org/10.1002/mrm.24488) PMID: [23001828](https://pubmed.ncbi.nlm.nih.gov/23001828/)
7. McGill LA, Ismail TF, Nielles-Vallespin S, Ferreira P, Scott AD, Roughton M, et al. Reproducibility of in vivo diffusion tensor cardiovascular magnetic resonance in hypertrophic cardiomyopathy. *J Cardiovasc Magn Reson* 2012; 14: 86. doi: [10.1186/1532-429X-14-86](https://doi.org/10.1186/1532-429X-14-86) PMID: [23259835](https://pubmed.ncbi.nlm.nih.gov/23259835/)
8. Tunnicliffe EM, Scott AD, Ferreira P, Ariga R, McGill LA, Nielles-Vallespin S, et al. Intercentre reproducibility of cardiac apparent diffusion coefficient and fractional anisotropy in healthy volunteers. *J Cardiovasc Magn Reson* 2014; 16: 31. doi: [10.1186/1532-429X-16-31](https://doi.org/10.1186/1532-429X-16-31) PMID: [24886285](https://pubmed.ncbi.nlm.nih.gov/24886285/)
9. Bulkley BH, Weisfeldt ML, Hutchins GM. Asymmetric septal hypertrophy and myocardial fiber disarray. Features of normal, developing and malformed hearts. *Circulation* 1977; 56: 292–8. PMID: [141348](https://pubmed.ncbi.nlm.nih.gov/141348/)
10. Maron BJ, Roberts WC. Quantitative analysis of cardiac muscle cell disorganization in the ventricular septum of patients with hypertrophic cardiomyopathy. *Circulation* 1979; 59: 689–706. PMID: [570464](https://pubmed.ncbi.nlm.nih.gov/570464/)
11. Maron BJ, Anan TJ, Roberts WC. Quantitative analysis of the distribution of cardiac muscle cell disorganization in the left ventricular wall of patients with hypertrophic cardiomyopathy. *Circulation* 1981; 63: 882–94. PMID: [7193536](https://pubmed.ncbi.nlm.nih.gov/7193536/)
12. Tseng WI, Dou J, Reese TG, Wedeen VJ. Imaging myocardial fibre disarray and intramural strain hypokinesia in hypertrophic cardiomyopathy with MRI. *J Magn Reson Imaging* 2006; 23: 1–8. PMID: [16331592](https://pubmed.ncbi.nlm.nih.gov/16331592/)
13. Moseley ME, Cohen Y, Kucharczyk J. Diffusion-weighted MR imaging of anisotropic water diffusion in cat central nervous system. *Radiology* 1990; 176: 439–46. PMID: [2367658](https://pubmed.ncbi.nlm.nih.gov/2367658/)
14. Basser PJ, Mattiella J, LeBihan D. MR Diffusion Tensor spectroscopy and imaging. *Biophysical Journal* 1994; 66: 259–67. PMID: [8130344](https://pubmed.ncbi.nlm.nih.gov/8130344/)
15. Basser PJ. Inferring microstructural features and the physiological state of tissues from diffusion-weighted images. *NMR Biomed* 1995; 8: 333–44. PMID: [8739270](https://pubmed.ncbi.nlm.nih.gov/8739270/)
16. Hsu EW, Muzikant SA, Matulevicius RC. Magnetic resonance myocardial fibre-orientation mapping with direct histological correlation. *Am J Physiol Heart Circ Physiol* 1998; 274: H1627–34.
17. Scollan DF, Holmes A, Winslow R, Forder JI. Histological validation of myocardial microstructure obtained from diffusion tensor magnetic resonance imaging. *Am J Physiol Heart Circ Physiol* 1998; 275: H2308–18.
18. Holmes AA, Scollan DF, Winslow RL. Direct histological validation of diffusion tensor MRI in formaldehyde-fixed myocardium. *Magn Res Med* 2000; 44: 157–61.
19. Tseng WY, Wedeen VJ, Reese TG, Smith RN, Halpern EF. Diffusion tensor MRI of myocardial fibers and sheets: correspondence with visible cut-face texture. *J Magn Reson Imaging* 2003; 17: 31–42. PMID: [12500272](https://pubmed.ncbi.nlm.nih.gov/12500272/)
20. Reese TG, Wedeen VL, Weisskoff RM. Measuring diffusion in the presence of material strain. *J Magn Reson* 1996; Series B 112: 253–8.
21. Tseng WI, Reese TG, Weisskoff RM, Wedeen VJ. Cardiac diffusion tensor MRI in vivo without strain correction. *Magn Reson Med* 1999; 42: 393–403. PMID: [10440965](https://pubmed.ncbi.nlm.nih.gov/10440965/)
22. Dou J, Reese TG, Tseng WI, Wedeen VJ. Cardiac diffusion MRI without motion effects. *Magn Reson Med* 2002; 48: 105–14. PMID: [12111937](https://pubmed.ncbi.nlm.nih.gov/12111937/)
23. Delattre BM, Viallon M, Wei H, Zhu YM, Feiweier T, Pai VM, et al. In vivo cardiac diffusion-weighted magnetic resonance imaging: quantification of normal perfusion and diffusion coefficients with intravoxel incoherent motion imaging. *Invest Radiol* 2012; 47: 662–70. doi: [10.1097/RLI.0b013e31826ef901](https://doi.org/10.1097/RLI.0b013e31826ef901) PMID: [23001045](https://pubmed.ncbi.nlm.nih.gov/23001045/)
24. Callot V, Bennett E, Decking UKM, Balaban RS, Wen H. In vivo study of microcirculation in canine myocardium using the IVIM method. *Magn Reson Med* 2003; 50: 531–40. PMID: [12939761](https://pubmed.ncbi.nlm.nih.gov/12939761/)
25. Le Bihan D, Breton E, Lallemand D, Aubin ML, Vignaud J, Laval-Jeantet M. Separation of diffusion and perfusion in intravoxel incoherent motion MR imaging. *Radiology* 1988; 168: 497–505. PMID: [3393671](https://pubmed.ncbi.nlm.nih.gov/3393671/)
26. Scott AD, Ferreira PF, Nielles-Vallespin S, Gatehouse P, McGill LA, Kilner P, et al. Optimal diffusion weighting for In vivo cardiac diffusion tensor imaging. *Magn Reson Med* 2014; Aug 22. (E-pub before print) doi: [10.1002/mrm.25418](https://doi.org/10.1002/mrm.25418)

27. Angeli S, Befera N, Peyrat JM, Calabrese E, Johnson GA, Constantinides C. A high-resolution cardiovascular magnetic resonance diffusion tensor map from ex-vivo C57BL/6 murine hearts. *J Cardiovasc Magn Reson*. 2014 Oct 16; 16(1):77.
28. Jiang Y, Guccione JM, Ratcliffe MB, Hsu EW. Transmural heterogeneity of diffusion anisotropy in the sheep myocardium characterized by MR diffusion tensor imaging. *Am J Physiol Heart Circ Physiol* 2007; 293: H2377–84. PMID: [17604331](#)
29. Helm PA, Tseng HJ, Younes L, McVeigh ER, Winslow RL. Ex vivo 3D diffusion tensor imaging and quantification of cardiac laminar structure. *Magn Reson Med* 2005; 54: 850–9. PMID: [16149057](#)
30. Griswold MA, Jakob PM, Heidemann RM, Nittka M, Jellus V, Wang J, et al. Generalized autocalibrating partially parallel acquisitions (GRAPPA). *Magn Reson Med* 2002; 47: 1202–10. PMID: [12111967](#)
31. Guizar-Sicairos M, Thurman ST, Fienup JR. Efficient subpixel image registration algorithms. *Optics letters* 2008; 33: 156–8. PMID: [18197224](#)
32. Kingsley PB. Introduction to diffusion tensor imaging mathematics: part III. Tensor calculation, noise, simulations, and optimization. *Concepts Magn Reson*. 2006; 28A: 155–79.
33. Bammer R, Holdsworth SJ, Veldhuis WB, Skare ST. New methods in diffusion-weighted and diffusion tensor imaging. *Magn Reson Imaging Clin N Am* 2009; 17: 175–204. doi: [10.1016/j.mric.2009.01.011](#) PMID: [19406353](#)
34. Wu EX, Wu Y, Nicholls JM, Wang J, Liao S, Zhu S, et al. MR diffusion tensor imaging study of postinfarct myocardium structural remodeling in a porcine model. *Magn Reson Med* 2007; 58: 687–95. PMID: [17899595](#)
35. Lombaert H, Peyrat JM, Croisille P, Rapacchi S, Fanton L, Cheriet F, et al. Human atlas of the cardiac fiber architecture: study on a healthy population. *IEEE Trans Med Imaging* 2012; 31: 1436–47. doi: [10.1109/TMI.2012.2192743](#) PMID: [22481815](#)
36. Reeder SB, Wintersperger BJ, Dietrich O, Lanz T, Greiser A, Reiser MF, et al. Practical approaches to the evaluation of signal-to-noise ratio performance with parallel imaging: application with cardiac imaging and a 32-channel cardiac coil. *Magn Reson Med* 2005; 54: 748–54. PMID: [16088885](#)
37. Benson AP, Bernus O, Dierckx H, Gilbert SH, Greenwood JP, Holden AV, et al. Construction and validation of anisotropic and orthotropic ventricular geometries for quantitative predictive cardiac electrophysiology. *Interface Focus* 2011; 1: 101–16. doi: [10.1098/rsfs.2010.0005](#) PMID: [22419977](#)
38. Nielles-Vallespin S, Mekkaoui C, Gatehouse P, Reese TG, Keegan J, Ferreira PF, et al. Erratum to in vivo diffusion tensor MRI of the human heart: reproducibility of breath-hold and navigator-based approaches (*Magn Reson Med* 2013; 70: 454–65). *Magn Reson Med* 2014; 72: 599. doi: [10.1002/mrm.25237](#)
39. Streeter DD Jr, Spotnitz HM, Patel DP, Ross J Jr, Sonnenblick EH. Fiber orientation in the canine left ventricle during diastole and systole. *Circ Res* 1969; 24: 339–47. PMID: [5766515](#)
40. Greenbaum RA, Ho SY, Gibson DG, Becker AE, Anderson RH. Left ventricular fibre architecture in man. *Br Heart J* 1981; 45: 248–63. PMID: [7008815](#)
41. Healy LJ, Jiang Y, Hsu EW. Quantitative comparison of myocardial fiber structure between mice, rabbit, and sheep using diffusion tensor cardiovascular magnetic resonance. *J Cardiovasc Magn Reson* 2011; 13: 74. doi: [10.1186/1532-429X-13-74](#) PMID: [22117695](#)
42. LeGrice IJ, Takayama Y, Covell JW. Transverse shear along myocardial cleavage planes provides a mechanism for normal systolic wall thickening. *Circ Res* 1995; 77: 182–93. PMID: [7788876](#)
43. Rademakers FE, Rogers WJ, Guier WH, Hutchins GM, Siu CO, Weisfeldt ML, et al. Relation of regional cross-fiber shortening to wall thickening in the intact heart. Three-dimensional strain analysis by NMR tagging. *Circulation* 1994; 89: 1174–82. PMID: [8124804](#)
44. LeGrice IJ, Smaill BH, Chai LZ, Edgar SG, Gavin JB, Hunter PJ. Lamina structure of the heart: ventricular myocyte arrangement and connective tissue architecture in the dog. *Am J Physiol* 1995; 269: H571–82. PMID: [7653621](#)
45. Gilbert SH, Benoist D, Benson AP, White E, Tanner SF, Holden AV, et al. Visualization and quantification of whole rat heart laminar structure using high-spatial resolution contrast-enhanced MRI. *Am J Physiol Heart Circ Physiol*. 2012 Jan 1; 302:H287–98. doi: [10.1152/ajpheart.00824.2011](#) PMID: [22021329](#)
46. Arts T, Costa KD, Covell JW, McCulloch AD. Relating myocardial laminar architecture to shear strain and muscle fiber orientation. *Am J Physiol Heart Circ Physiol* 2001; 280: H2222–9. PMID: [11299225](#)
47. Hooks DA, Trew ML, Caldwell BJ, Sands GB, LeGrice IJ, Smaill BH. Lamina arrangement of ventricular myocytes influences electrical behavior of the heart. *Circ Res*. 2007 Nov 9; 101:e103–12. PMID: [17947797](#)
48. Waldman LK, Nosan D, Villarreal F, Covell JW. Relation between transmural deformation and local myofiber direction in canine left ventricle. *Circ Res* 1988; 63: 550–62. PMID: [3409487](#)

49. McGill LA, Ferreira P, Scott AD, Nielles-Vallespin S, Silva R, Kilner PJ, et al. Abstract: Comparison of cardiac DTI parameters between systole and diastole (abstract). *J Cardiovasc Magn Reson* 2014; 16 (Suppl 1): P39.
50. Dou J, Tseng WY, Reese TG, Wedeen VJ. Combined diffusion and strain MRI reveals structure and function of human myocardial laminar sheets in vivo. *Magn Reson Med* 2003; 50:107–13. PMID: [12815685](#)
51. Ferreira PF, Kilner PJ, McGill LA, Nielles-Vallespin S, Scott AD, Ho YS, et al. In vivo cardiovascular magnetic resonance diffusion tensor imaging shows evidence of abnormal myocardial laminar orientations and mobility in hypertrophic cardiomyopathy. *J Cardiovasc Magn Reson* 2014; 16: 87. doi: [10.1186/s12968-014-0087-8](#) PMID: [25388867](#)
52. Axel L, Wedeen VJ, Ennis DB. Probing dynamic myocardial microstructure with cardiac magnetic resonance diffusion tensor imaging. *J Cardiovasc Magn Reson* 2014; 16: 89. doi: [10.1186/s12968-014-0089-6](#) PMID: [25388937](#)
53. Stoeck CT, Kalinowska A, von Deuster C, Harmer J, Chan RW, Niemann M et al. Dual-Phase Cardiac Diffusion Tensor Imaging with Strain Correction. *PLoS ONE* 2014; 9: e107159. doi: [10.1371/journal.pone.0107159](#) PMID: [25191900](#)
54. Jones DK, Basser PJ. "Squashing peanuts and smashing pumpkins": how noise distorts diffusion-weighted MR data. *Magn Reson Med* 2004; 52: 979–93. PMID: [15508154](#)
55. Pierpaoli C, Basser PJ. Toward a quantitative assessment of diffusion anisotropy. *Magn Reson Med*. 1996; 36: 893–906. PMID: [8946355](#)
56. Koh DM, Thoeny HC. *Diffusion weighted MR imaging*. Springer, 2010. ISBN 978-3-540-78576-7.